EUROPHYSICS LETTERS 1 April 1994

Europhys. Lett., **(26)** (1), pp. 37-42 (1994)

Optical Binding in Scanning Probe Microscopy.

A. DEREUX (*), C. GIRARD (**), O. J. F. MARTIN (***) and M. DEVEL (**)

(*) *Institute for Studies in Interface Sciences*
Facultés Universitaires Notre-Dame de la Paix
Rue de Bruxelles 61, B-5000 Namur, Belgium
(**) *Laboratoire de Physique Moléculaire, UA CNRS 772,*
Université de Franche Comté - F-25030 Besançon Cedex, France
(***) *IBM Research Division, Zurich Research Laboratory*
Säumerstrasse 4, CH-8803 Rüschlikon, Switzerland

(received 22 November 1993; accepted in final form 3 February 1994)

PACS. 61.16D – Electron microscopy determinations.

Abstract. – When a light beam impinges on two interacting objects of subwavelength size, a spatially confined electromagnetic field arises in the immediate proximity of the particles. In scanning probe microscopy, short-range forces induced by this electromagnetic near-field change the magnitude of the probe tip-substrate interaction. In this letter we analyse the physical process responsible for these forces in the context of the localized field susceptibility method.

Introduction. – When a laser beam is focused on the gap between the probe tip of a scanning microscope and a sample surface, various physical phenomena are expected [1-3]. As described in ref. [3], the light absorbed by the tip and the sample may provoke a thermal expansion of the system leading to a possible optical absorption spectroscopy of the sample. The electric field associated with the incident light beam can also produce an additional force between the probe tip and the substrate. This force is expected as a result of light pressure effects. Indeed, various experiments like atomic-cooling devices [4] or optical traps [5] demonstrated that radiation pressure effects give rise to significant forces not only on atoms but also on micrometre-sized particles. Moreover, it was recently proved that multiple scattering of light between two sufficiently close objects is able to induce an optical binding force between the two objects [6, 7].

Questions concerning the possible use of this kind of inductive effect between a probe tip and a sample surface arose in the context of scanning tunnelling optical microscopy (STOM) (also called photon scanning tunnelling microscopy (PSTM)) [8-12]. Rough numerical estimations [7] indicated that the order of magnitude of this inductive force should be experimentally accessible. However, the magnitude and the spatial behaviour of such forces as a function of photon energy, tip-sample distance and other geometrical and material parameters of both the probe and the surface have not yet been described accurately.

In recent articles [7, 13], we developed a theoretical approach to study the main features of the physical interaction between an elongated probe tip and a corrugated surface. These studies were based on self-consistent calculations of the coupling modes of two interacting systems in the context of the localized field susceptibility method [14]. In this paper, we apply this formalism to the calculation of the field distribution inside and around the

tip-sample junction. In this analytical framework, we derive a general expression for the tip-sample force induced by the incident light. We will present numerical simulations of this optical binding force to illustrate our discussion of the parameters required in order to allow experimental observation.

Coupled modes of the tip-sample system. – Applying an external time-harmonic field $\boldsymbol{E}_0(\boldsymbol{r}, \omega)$ (*e.g.* a laser beam) to the tip-sample junction of a scanning microscope creates an electric field $\boldsymbol{E}(\boldsymbol{r}, \omega)$ in the vicinity of the interfaces. To obtain the new field distribution $\boldsymbol{E}(\boldsymbol{r}, \omega)$ inside the probe-sample system, one needs to solve the implicit integral equation

$$\boldsymbol{E}(\boldsymbol{r}, \omega) = \boldsymbol{E}_0(\boldsymbol{r}, \omega) + \int \mathrm{d}\boldsymbol{r}' \, \boldsymbol{S}(\boldsymbol{r}, \boldsymbol{r}', \omega) \cdot \chi_\mathrm{p}(\boldsymbol{r}', \omega) \cdot \boldsymbol{E}(\boldsymbol{r}', \omega), \tag{1}$$

where the integral extends over the volume occupied by the tip (cf. fig. 1) and $\chi_\mathrm{p}(\boldsymbol{r}', \omega)$ describes its linear susceptibility. The close tip-sample distance (assumed to be 5 nm in the simulations to be detailed below) will lead to strong interaction between the tip and the sample surface. Therefore the sample response must be properly taken into account. In our procedure, this response is accurately contained in $\boldsymbol{S}(\boldsymbol{r}, \boldsymbol{r}', \omega)$ which is the propagator associated with a plane surface system. We use for $\boldsymbol{S}(\boldsymbol{r}, \boldsymbol{r}', \omega)$ the rather elaborate derivation that can be found in ref. [14]. $\boldsymbol{S}(\boldsymbol{r}, \boldsymbol{r}', \omega)$ is defined like a Green's function: it determines the electromagnetic response at $\boldsymbol{r}$ due to a point source located at $\boldsymbol{r}'$. If one assumes that the probe tip is made of a material that responds locally, a space discretization procedure [7, 13] leads to the following set of linearly coupled equations ($\boldsymbol{I}$ is the unit dyadic):

$$\sum_{j=1}^{m} [\boldsymbol{I}\delta_{ij} - \boldsymbol{S}(\boldsymbol{r}_i, \boldsymbol{r}_j, \omega) \cdot \chi_\mathrm{p}(\boldsymbol{r}_j, \omega) w_j] \cdot \boldsymbol{E}(\boldsymbol{r}_i, \omega) = \boldsymbol{E}_0(\boldsymbol{r}_j, \omega) \qquad (i = 1, m), \tag{2}$$

where m represents the number of points used to discretize the probe tip and w_j is the integration weight attributed to the j-th discretization cell. Note that both i and j run over meshes located inside the probe tip. Discretization cells outside the tip are not necessary since, thanks to the Huygens-Fresnel principle, the field distribution inside the tip and the propagator $\boldsymbol{S}(\boldsymbol{r}, \boldsymbol{r}', \omega)$ are sufficient to describe the electric field anywhere else. Indeed, if $\boldsymbol{R}$ is an arbitrary vector, eq. (1) yields

$$\boldsymbol{E}(\boldsymbol{R}, \omega) = \boldsymbol{E}_0(\boldsymbol{R}, \omega) + \sum_{j=1}^{m} \boldsymbol{S}(\boldsymbol{R}, \boldsymbol{r}_j, \omega) \cdot \chi_\mathrm{p}(\boldsymbol{r}_j, \omega) \cdot \boldsymbol{E}(\boldsymbol{r}_j, \omega) w_j \, . \tag{3}$$

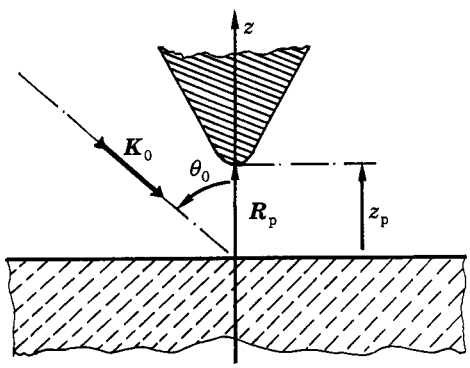

Fig. 1. – Geometry of an experimental scanning probe device illuminated in external reflection. The wave vector $\boldsymbol{K}_0$ is located in the (y, x)-plane and θ is the angle of incidence. The vector $\boldsymbol{R}_\mathrm{p} = (x_\mathrm{p}, y_\mathrm{p}, z_\mathrm{p})$ points to the apex of the probe tip.

We note that the above procedure avoided the matching of boundary conditions which was implicitly satisfied by the self-consistency of eq. (1). Since the inversion required by eq. (2) is exact for a given discretization grid, the only approximation lies in the density of cells used to describe the probe tip.

The tip-sample force in the non-contact regime. – When the probing tip approaches the surface but is kept high enough above the surface so that the electrons wave functions do not overlap, the long-range interaction energy $U(z_p)$ includes the two terms of virtual and real photons (provided that no permanent charge exists):

$$U(z_p) = U_{vdW}(z_p) + U_{ind}(z_p), \tag{4}$$

where z_p is the distance from the probe apex to the sample surface (fig. 1). The interaction energy of virtual photons in the van der Waals dispersion energy $U_{vdW}(z_p)$ originating from the correlation between the fluctuations of the charges densities inside the probe tip and the substrate [14]. The contribution of real photons constitutes the optical binding energy $U_{ind}(z_p)$ induced by the incident light beam. The calculation of the latter quantity requires that the spatial and temporal form of the external field $\boldsymbol{E}_0(\boldsymbol{r}, t)$ be specified. As stated above, the present article is restricted to the case of a time-harmonic field of frequency ω. The time-dependent electrical polarization at any point $\boldsymbol{r}$ inside the tip-sample junction is then given by

$$\boldsymbol{P}_\alpha(\boldsymbol{r}, t) = \mathrm{Re}[\chi_\alpha(\boldsymbol{r}, \omega)\boldsymbol{E}(\boldsymbol{r}, \omega) \exp[-i\omega t], \tag{5}$$

where the index α takes the values p and s in the probe and the substrate, respectively. Note that, in eqs. (2) and (3), $\boldsymbol{P}_\alpha(\boldsymbol{r}, t)$ is a functional of the incident field. When this incident field increases from zero to a finite value, the system acquires the following time-averaged light inductive energy:

$$U_{ind}(z_p) = U_s(z_p) + U_p(z_p). \tag{6}$$

The force normal to the surface is computed by differentiating the light inductive energy:

$$F_z = -\frac{\partial U_{ind}}{\partial z_p}. \tag{7}$$

The first term in eq. (6), $U_s(z_p)$, describes the time-averaged inductive energy experienced by the sample and is obtained by integration over the semi-infinite substrate ($\chi_s(\boldsymbol{r}, \omega)$ is the linear susceptibility of the substrate):

$$U_s(z_p) = -\frac{1}{4}\int_{-\infty}^{+\infty} dx \int_{-\infty}^{+\infty} dy \int_{-\infty}^{0} dz\, \chi_s(\boldsymbol{r}, \omega)|\boldsymbol{E}(\boldsymbol{r}, \omega)|^2. \tag{8}$$

The convergence of this integral will be assessed in the next section. The second term $U_p(z_p)$ in eq. (6) includes the time-averaged inductive energy associated with the probe tip. This quantity may be expanded on the discretization grid used in eq. (2):

$$U_p(z_p) = -\frac{1}{4}\sum_{j=1}^{m} w_j \chi_p(\boldsymbol{r}_j, \omega)|\boldsymbol{E}(\boldsymbol{r}_j, \omega)|^2. \tag{9}$$

Before we consider numerical results in detail, let us discuss the case where the matrix $[\boldsymbol{I}\delta_{ij} - \boldsymbol{S}(\boldsymbol{r}_i, \boldsymbol{r}_j, \omega) \cdot \chi_p(\boldsymbol{r}_j, \omega) w_j]$ in eq. (2) becomes singular. For a fixed frequency, the determinant of this matrix vanishes if the tip-sample configuration displays resonances. In particular, for a pointed metallic tip above a metallic substrate, this resonance can occur in the optical range before the tip touches the sample surface. Such resonant effects have

recently been observed by generating localized plasmons on a spherical metallic probe tip approaching a surface. In the near-field zone (about 100 nm from the surface) extremely narrow resonance peaks *vs.* the approach distance were recorded [15]. Such gap modes could also generate specific resonance phenomena in the inductive force. This differs from the behaviour of van der Waals forces in which the integration on the imaginary frequencies damps resonance phenomena [14].

Application to specific configurations. – The essential component of any scanning probe microscope is the nanoprobe that records the relevant physical phenomena (*e.g.* tunnelling current, interacting forces, electromagnetic field) for a given spatial configuration. In the

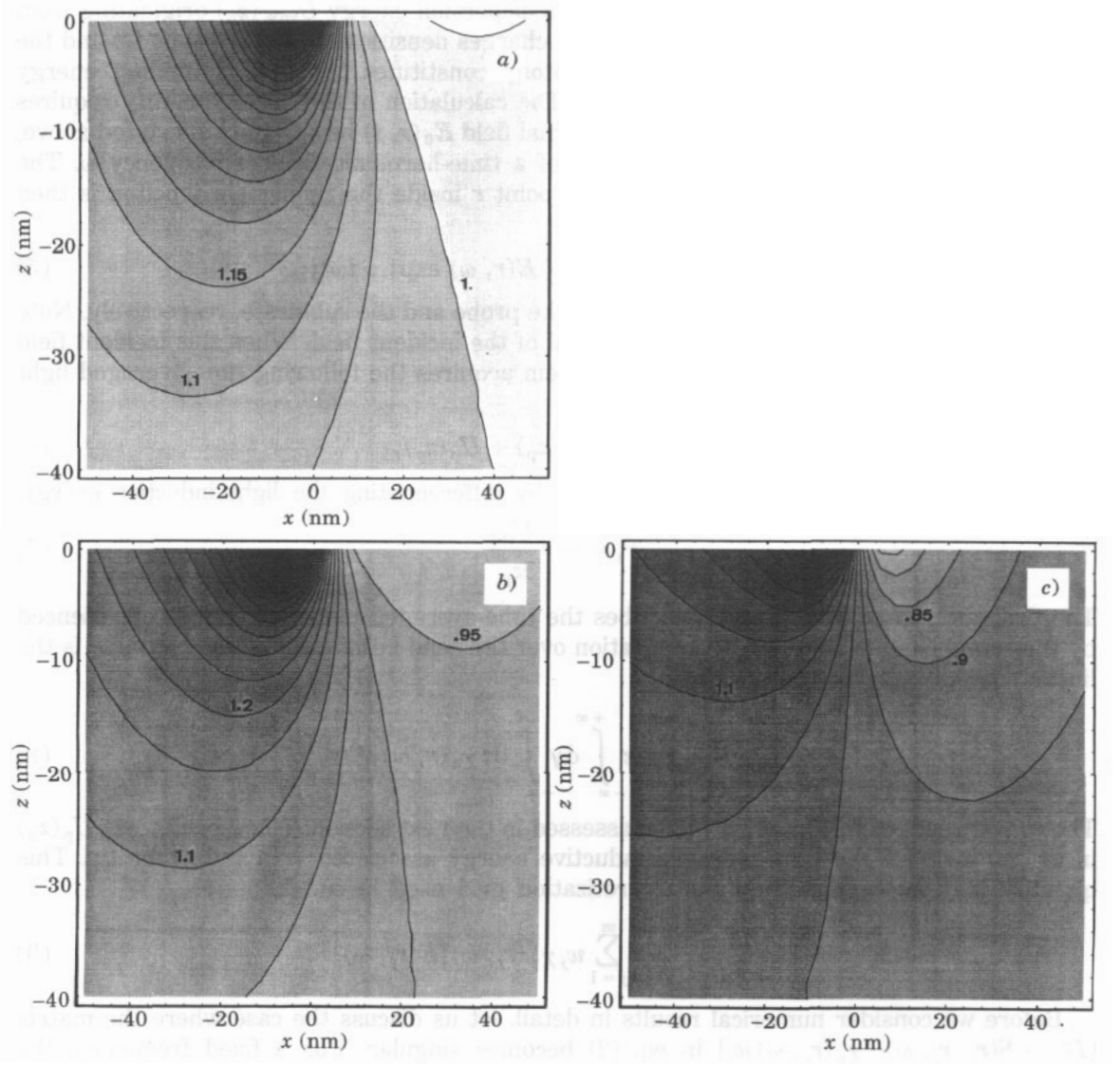

Fig. 2. – Three sequences of constant isointensity curves η in the plane $y = 0$ inside the substrate. The calculation was performed with a 100 nm high tetrahedral tip. The curvature radius of the tip end was 7.5 nm and the approach distance was $z_p = 5$ nm. *a*) $\theta = 85°$; *b*) $\theta = 60°$; *c*) $\theta = 30°$.

context of near-field experiments coupled with force sensor devices, two types of optical probes have already been investigated. One class of probes was obtained by mechanical pulling and chemical etching of both monomode or multimode optical fibres [16]. The other kind of tips were micro fabricated SiN pyramids integrated on micro cantilevers (currently used in SFM) [17]. Such probe tip consisted of a tetrahedrally shaped protrusion the four faces and the four sharp edges of which converge to an apex with a small curvature radius (typically between 1 and 50 nm). In our numerical application, we considered such a tetrahedral tip apex facing a perfectly plane surface (cf. fig. 1). The pyramid was 100 nm high and had an aperture angle of 90°. Its optical index n_p was varied between 1.5 and 2.5. This pyramid was discretized on a Cartesian grid obtained by stacking 6 layers of meshes on the sample surface. We restricted our application to the external reflection configuration described in fig. 1.

As described in the analytical developments above, the magnitude of the light-inductive energy depends on the magnitude of the self-consistent field $\boldsymbol{E}(\boldsymbol{r}, \omega)$ inside the tip and the sample. In order to characterize the spatial extension of this field, we calculated the normalized-electric field intensity $\eta = |\boldsymbol{E}(\boldsymbol{r}, \omega)|^2 / |\boldsymbol{E}_0(\boldsymbol{r}, \omega)|^2$ inside the substrate (fig. 2). We found that for an approach distance z_p of about 5 nm, a very confined field occurred in the gap. Introducing a tip with a curvature radius of 7.5 nm, the spatial width of η was usually less than 30 nm. In this configuration of external reflection, we also found that the shape of the intensity maps due to a p-polarized incident field depended dramatically on the angle of incidence θ. A possible origin of this effect is the shadow introduced by the probe in the near-field zone. This situation occurred preferentially for small angles of incidence. In any case these simulations illustrate in a striking way the optical confinement originating from the interface geometry. The assessment of the decay of η inside the substrate as the distance $|\boldsymbol{r} - \boldsymbol{R}_p|$ increased was essential to allow the numerical integration of the light-inductive energy inside the substrate (eq. (9)). The choice of an external illumination set-up in our simulations was the less favourable situation to optimize this aspect of the problem, since the incident field took the form of a reflected plane wave. The decay of η would be more

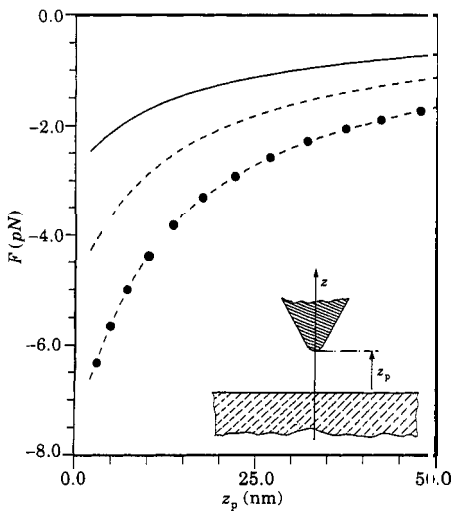

Fig. 3. – Variation of the normal light-inductive force as a function of the approach distance z_p. The calculation was performed in the vicinity of the Brewster angle with a 400 nm high tetrahedral tip terminated by a 30 nm curvature radius. Solid line: $n_p = 1.5$; dash line: $n_p = 2.0$; dashed-dotted line: $n_p = 2.5$.

convenient when simulating a STOM (or PSTM) set-up where the incident wave is decreasing exponentially from the sample surface.

Once the spatial distribution of the electric field was computed with eq. (2), it was possible to study numerically the behaviour of the optical binding force F_z. As in ref. [6], we assumed that the focused laser beam provided 2.2 W of mean power over a surface of 150 μm^2. For fixed horizontal coordinates ($x_p = 0$, $y_p = 0$), U_{ind} was computed for several points z_p along the vertical axis and fitted from these points with a polynomial in z_p. The vertical component of the force was then differentiated from this polynomial, thus allowing us to plot F_z as a function of the approach distance z_p as in fig. 3. In this figure, the calculation was performed near the Brewster angle ($\theta = 56.5°$) with a 400 nm high tetrahedral tip terminated by a curvature radius of 40 nm. The magnitude of the force varied within 2 and 6 pN when the tip was located in the immediate proximity of the sample. Such a force lies within the detection range of today's resonant SFM devices [17]. Since the efficiency of the optical binding force between the tip and the substrate is related to the confined character of the optical near-field, this phenomenon is exploitable for scanning microscopy.

Although we restricted our discussion to real optical properties, our procedure is able to take complex and anisotropic optical properties into account. Using absorbing or anisotropic material is expected to alter significantly the sign, magnitude and spatial dependence of the probe tip interaction. It will be worth considering such specific optical responses since the strong sensitivity of the magnitude of F_z with respect to the optical index of the probe tip (fig. 3) can open new perspectives for the realization of practical devices.

* * *

We thank D. COURJON, M. HIPP, O. MARTI and M. SPAJER for stimulating discussions. One of us (AD) gratefully acknowledges the Walloon Ministry for Research and Technology (Brussels) for financial support. This work was performed in the framework of the Human Capital and Mobility program initiated by the Commission of the European Community.

REFERENCES

[1] MARTI O. and BALYKIN V. I., in *Near Field Optics, NATO ser. E*, edited by D. W. POHL and D. COURJON (Kluwer, Dordrecht) 1993, p. 121, and references therein.
[2] MARTI O., RUF A., HIPP N., BIELEFEDT D., COLCHER J. and MLYNEK J., *Ultramicroscopy*, **42-44** (1992) 345.
[3] NONNENMACHER M. and WICKRAMASINGHE H. K., *Ultramicroscopy*, **42-44** (1992) 351.
[4] STENHOLM S., *Rev. Mod. Phys.*, **58** (1986) 699.
[5] ASHKIN A., *Science*, **210** (1980) 1081.
[6] BURNS M. M., FOURNIER J. M. and GOLOVCHENKO J. A., *Phys. Rev. Lett.*, **63** (1989) 1233.
[7] DEREUX A., VIGNERON J. P., LAMBIN PH. and LUCAS A. A., *Physica B*, **175** (1991) 65.
[8] DEPASSE F. and COURJON D., *Opt. Commun.*, **87** (1992) 79.
[9] FERRELL T. L., SHARP S. L. and WARMACK R. J., *Ultramicroscopy*, **42-44** (1991) 408.
[10] DE FORNEL F., SALOMON L., ADAM P., BOURILLOT E., GOUDONNET J. P. and NEVIERE M., *Ultramicroscopy*, **42-44** (1992) 422.
[11] SPECHT M., PEDARNIG J. D., HECKL W. M. and HANSH T. W., *Phys. Rev. Lett.*, **68** (1992) 496.
[12] PAESLER M. A., MOYER P. J., JAHNKE C. J., JOHNSON C. E., REDDICK R. C., WARMACK R. J. and FERRELL T. L., *Phys. Rev. B*, **42** (1990) 6750.
[13] GIRARD C., BOUJU X. and DEREUX A., in *Near Field Optics, NATO ser. E*, edited by D. W. POHL and D. COURJON (Kluwer, Dordrecht) 1993, p. 199.
[14] GIRARD C. and BOUJU X., *J. Chem. Phys.*, **95** (1991) 2056.
[15] FISCHER U. CH. and POHL D. W., *Phys. Rev. Lett.*, **62** (1989) 458.
[16] COURJON D., SARAYEDDINE K. and SPAJER M., *Opt. Commun.*, **71** (1989) 23.
[17] SARID D., *Scanning Force Microscopy* (Oxford University Press, Oxford) 1991.